Clipping Distortion Suppression of Directly Modulated Multi-IF-over-Fiber Mobile Fronthaul Links Using Shunt Diode Predistorter

Changyo Han, Seung-Hyun Cho, Minkyu Sung, Hwan Seok Chung, and Jong Hyun Lee

Herein, we demonstrate clipping distortion suppression of directly modulated multi-IF-over-fiber links using a simple shunt diode predistorter. The dynamic range of a directly modulated analog fiber optic link is limited by nonlinear distortions caused by laser-diode clipping. We investigate the link performance in the context of carrier-to-noise and distortion ratio (CNDR) and error vector magnitude (EVM) requirements when supporting LTE-A services. We also design an analog predistorter with a shunt-diode structure, and demonstrate experimentally that the predistorter has the ability to suppress clipping-induced third-order intermodulation distortions of the link by at most 14 dB. It also improves the CNDR and EVM of the 4-IF-multiplexed LTE-A carriers by 7 dB and 2.9%, respectively.

Keywords: Mobile fronthaul, LTE-A, radio-over-fiber, analog predistorter.

I. Introduction

Traffic demand in wireless networks is rapidly increasing owing to the use of various kinds of sophisticated mobile services and mobile devices. To reduce the capital expenditures and operational expenditures of mobile access networks, service providers have introduced the centralized radio access network (C-RAN) architecture [1]. In the C-RAN architecture, multiple remote radio units (RUs) are connected to a centralized baseband digital unit (DU) through the Common Public Radio Interface (CPRI) [2] or Open Base Station Architecture Initiative (OBSAI) [3], which are digital transmission protocols. In general, CPRI and OBSAI require a much larger bandwidth than that of transmitted radio frequency (RF) signals because they utilize a high quantization resolution for the digitization process [4], [5]. For instance, according to the CPRI specifications, a DU has to accommodate 58.9 Gb/s of data traffic per RU to provide a Long-Term Evolution Advanced (LTE-A) service exploiting a 20 MHz bandwidth, two carrier aggregations, three sectors, and an 8 × 8 multiple-input and multiple-output (MIMO) configuration, whereas the actual occupied bandwidth of the RF signals is 960 MHz [4].

To meet such traffic demands, several bandwidth-efficient and cost-effective mobile fronthaul architectures employing directly modulated multiple intermediate frequency-over-fiber (IFoF) schemes have recently been proposed [4]–[8]. These are very attractive approaches for current and upcoming mobile access networks because RF signals are transparently transported

Manuscript received Aug. 17, 2015; revised Feb. 19, 2016; accepted Mar. 2, 2016.

This work was supported by the IT R&D programs of MSIP (Ministry of Science, ICT and Future Planning), Korea (16ZI1310, Development of compact radio & dense digital base station technologies based on RoF for mobile communication systems).

Changyo Han (corresponding author, hanc@etri.re.kr), Seung-Hyun Cho (shc@etri.re.kr), Minkyu Sung (smk9620@etri.re.kr), Hwan Seok Chung (chung@etri.re.kr), and Jong Hyun Lee (jlee@etri.re.kr) are with Hyper-connected Communication Research Laboratory, ETRI, Daejeon, Rep. of Korea.

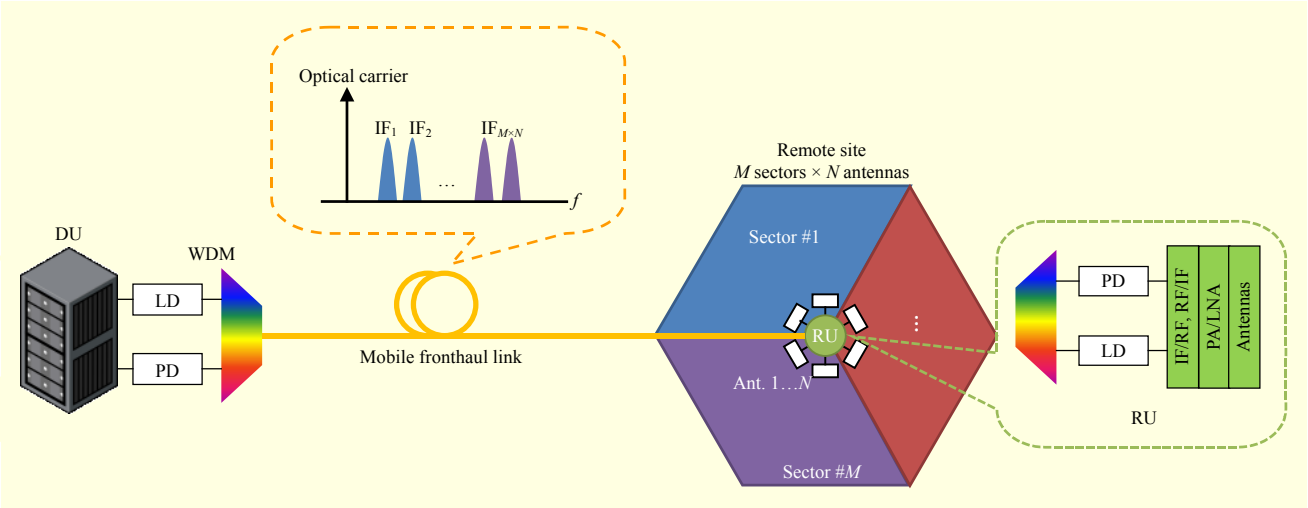

Fig. 1. Mobile fronthaul architecture employing multi-IFoF technique.

without increasing the occupied bandwidth. A typical configuration of a multi-IFoF-based mobile fronthaul is shown in Fig. 1. The DU is connected to the RU through an optical fiber cable. Assuming that an RU covers M sectors with N antennas per sector, RF signals of the antennas are mapped onto $M \times N$ IF carriers in a radio-over-fiber (RoF) link. The DU can accommodate multiple RUs with a single optical fiber by employing a wavelength-division multiplexing (WDM) technique.

Although a mobile fronthaul architecture using a multi-IFoF technique saves bandwidth resources and cost, the transmission capacity of such systems is limited by laser diode (LD)–inherent nonlinear distortions (NLDs) [9]–[12]. Moreover, the quality of LTE-A signals is severely degraded by such distortions compared to single-carrier modulation signals owing to the high peak-to-average power ratio characteristics of typical orthogonal frequency-division multiplexing signals [13].

It is known that the dominant distortion is clipping distortion in a directly modulated fiber-optic system [11]. There have been several attempts to compensate for a signal degradation arising from NLDs in directly modulated RoF systems. Feed-forward linearization methods show an admirable NLD suppression performance; however, these schemes are not easily implemented, because of their bulky and complex structures [14], [15]. Digital predistortion also requires sophisticated digital signal processing for implementation [16].

In this paper, we analyze the performance limitations of a multi-IFoF-based mobile fronthaul link by considering the analog fiber-optic link noise characteristics and clipping phenomenon.

Next, we describe the design of a simple, cost-effective analog predistorter based on a shunt diode structure and its impact on the transmission performance of analog fiber-optic links [17]. Finally, we demonstrate an analog predistorter in a mobile fronthaul fiber-optic link supporting a 4-IF carrier-multiplexed LTE-A signal.

II. Performance Limits of Multi-IFoF LTE-A Mobile Fronthaul Link

The 3rd Generation Partnership Project (3GPP) defines the maximum error vector magnitude (EVM) specifications of an LTE-A signal with 64-quadrature amplitude modulation (QAM) as 8.0% [18]. Although the EVM is a direct indicator of the quality of a modulated signal, an LTE-A demodulator is required for EVM measurements, because it should be conducted on baseband signals. Instead, we introduce a carrier-to-noise and distortion ratio (CNDR) measurement into traditional cable networks: the CNDR is defined as the sum of the carrier-to-noise ratio (CNR) and the carrier-to-distortion ratio. We assume that the CNDR of an LTE-A signal is similar to the signal-to-noise ratio (SNR) of the signal, because a CNDR measurement is conducted in the frequency domain. The relationship between the SNR and EVM can be described through the following equation [19]:

$$\mathrm{SNR\ (dB)} = -20\log_{10}\left(\frac{\mathrm{EVM\ (\%)}}{100}\right). \quad (1)$$

Figure 2 shows the relationship between the EVM and the CNDR and between the EVM and SNR. The solid line represents the SNR curve obtained from (1), and the round symbols indicate the experimentally measured CNDR curve using a 64-QAM LTE-A signal. We generated 20 MHz 64-QAM LTE-A signals using a vector signal generator (VSG), and measured the CNDR with an electrical spectrum analyzer

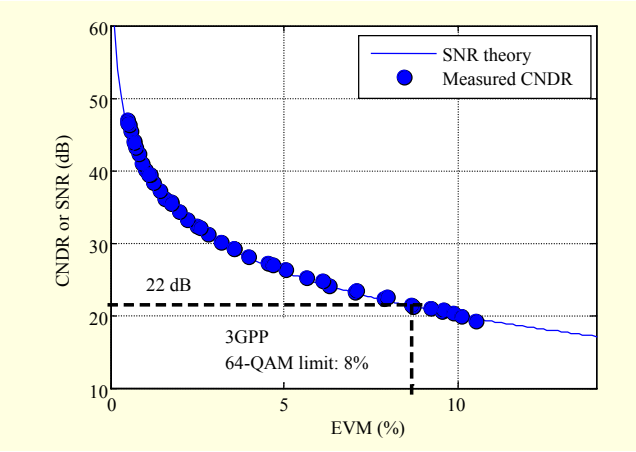

Fig. 2. Theoretical SNR calculated from EVM (solid line) and experimentally measured CNDR of 64-QAM LTE-A signal (round symbols).

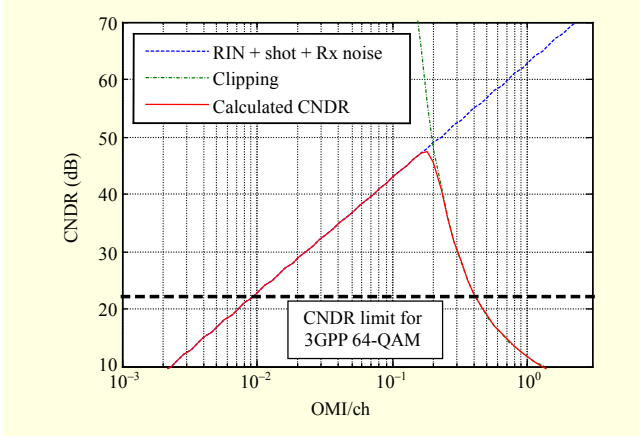

Fig. 3. CNDR as function of OMI/ch considering various noise and distortion terms of RoF link. Number of IF carriers = 4, signal bandwidth = 18.015 MHz, RIN = –155 dB/Hz, LD output power = 3 dBm, received optical power = –7 dBm, PD responsivity = 0.9 A/W, and receiver noise = 2×10^{-11} A/Hz$^{1/2}$.

(ESA). We can see a good agreement between the CNDR and SNR curves, which suggests that we can estimate the signal quality of an LTE-A signal through a spectrum measurement without the use of LTE-A demodulators. Considering the 3GPP 64-QAM EVM limit of 8%, the required CNDR obtained for LTE-A 64-QAM signals may be 22 dB.

We analyzed the performance limits of a directly modulated multi-IFoF link by calculating the CNDR of each IF carrier at the optical receiver, which can be expressed as [12]

$$\mathrm{CNDR}^{-1} = \mathrm{CNR}_{\mathrm{RIN}}{}^{-1} + \mathrm{CNR}_{\mathrm{shot}}{}^{-1} + \mathrm{CNR}_{\mathrm{Rx}}{}^{-1} + \mathrm{CDR}_{\mathrm{clipping}}{}^{-1}. \quad (2)$$

We considered three noise terms and one NLD term in (2). The first three terms on the right of the equation represent the CNRs based on the relative intensity noise (RIN), shot noise, and receiver noise, respectively. The last term represents the NLDs caused by LD clipping. These terms can be written as

$$\mathrm{CNR}_{\mathrm{RIN}} = \frac{m^2}{2\mathrm{RIN} \cdot B}, \quad (3)$$

$$\mathrm{CNR}_{\mathrm{shot}} = \frac{m^2 I_{\mathrm{p}}}{4qB}, \quad (4)$$

$$\mathrm{CNR}_{\mathrm{Rx}} = \frac{m^2 I_{\mathrm{p}}{}^2}{2B\left\langle i_{\mathrm{Rx}}{}^2 \right\rangle}, \quad (5)$$

$$\mathrm{CDR}_{\mathrm{clipping}} = \frac{\sqrt{2\pi}(1+6\mu^2)}{\mu^3} \exp\left(\frac{1}{2\mu^2}\right), \quad (6)$$

where m is the optical modulation index (OMI), RIN is the relative intensity noise of the optical source, B is the signal bandwidth, I_{p} is the received photocurrent, q is the electrical charge, $\langle i_{\mathrm{Rx}}{}^2 \rangle$ is the thermal noise of the receiver, and μ is the root-mean-square modulation index, which can be described as

$$\mu = m\sqrt{\frac{N}{2}}, \quad (7)$$

where N is the number of IF carriers.

Figure 3 shows the CNDR affected by various noise and distortion terms versus OMI per channel (OMI/ch) when using a distribution feedback (DFB) laser as a light source. The number of IF carriers was four, assuming that the mobile base station exploits two sectors and has a 2 × 2 MIMO configuration. The signal bandwidth was 18.015 MHz considering a 20 MHz bandwidth LTE-A signal with full resource block allocation. The optical link loss was 10 dB, including 20 km single-mode fiber (SMF) and WDM couplers. The results show that the performance of this system is limited by noise terms when the OMI/ch is less than 18%, whereas the spurious components generated by clipping distortion become a dominant limiting factor when the OMI/ch exceeds this percentage. To satisfy the CNDR requirements shown in Fig. 2, the acceptable OMI/ch range is 1% to 40%. It can be assumed that the acceptable OMI/ch range can be extended by inhibiting the CNDR limitations from the clipping distortion.

III. Design of Shunt Diode Predistorter

Figure 4(a) shows the principle of predistortion. As discussed in the previous section, LD clipping in RoF links causes harmonic and intermodulation distortions, which degrade the signal quality and thus limit the CNDR of the link. Such nonlinearity can be suppressed by inserting a predistorter with

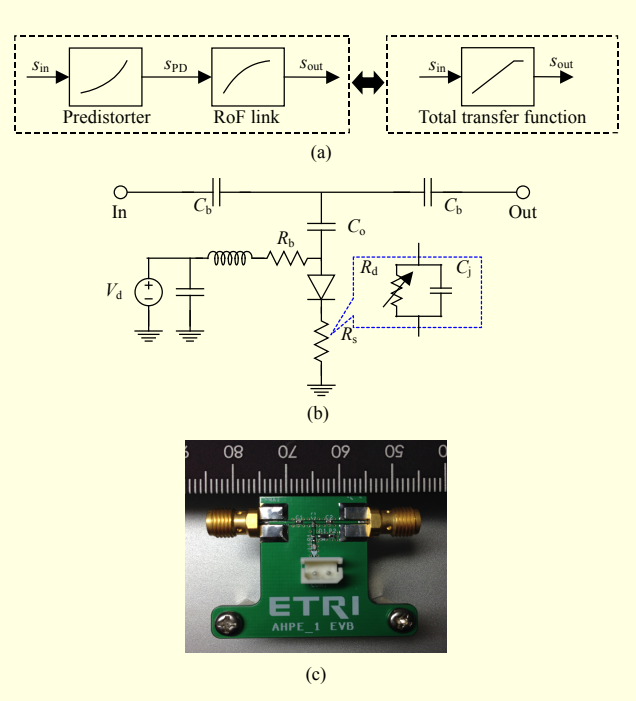

Fig. 4. (a) Principle of predistortion, (b) schematic diagram of designed predistortion circuit, and (c) implemented predistorter.

an inverse nonlinear response in front of the link [20].

A schematic diagram of the designed predistortion circuit is illustrated in Fig. 4(b). The circuit contains a shunt Schottky diode and passive electrical lumped components. A dc bias circuit with an RF choke applies bias current to the diode. The equivalent circuit of the RF Schottky diode is displayed in the dashed box above. It is a well-known fact that diode equivalent resistance, R_d, increases proportionally as the RF input power increases. To simplify the calculation, we assume a simplified equivalent circuit by excluding C_o and R_s gain. The gain and phase response of the circuit can be derived as [20]

$$|S_{21}| = \frac{2}{\sqrt{\left(2 + Z_o(R_d + R_b)/R_d \cdot R_b\right)^2 + \left(\omega C_j Z_o\right)^2}}, \quad (8)$$

$$\angle S_{21} = \tan^{-1}\left(-\frac{\omega C_j Z_o}{2 + Z_o(R_d + R_b)/R_d \cdot R_b}\right), \quad (9)$$

where Z_o is the characteristic impedance. From (8), we can find that the response of the predistortion circuit has a positive gain deviation and a negative phase deviation with an increase in R_d. We can tune the component values of C_o and R_s to accomplish an additional gain adjustment and impedance matching.

The nonlinearity of the RoF link was modeled from the AM-AM/PM response measured using a vector network analyzer (VNA) at 160 MHz. The values of the circuit components were carefully derived to remove third-order intermodulation distortion (IMD3) components by using the harmonic-balance method with AWRDE RF simulation software. First, we tuned R_b to optimize the response of the predistorter while monitoring the IMD suppression in the simulation, and then decided the values of the dc blocking capacitor, the source resistor, and other components to obtain proper impedance matching at the input and output ports. A BAS70 RF Schottky diode from NXP semiconductors was used for the predistortion circuit. The diode junction capacitance and other component values of the predistortion circuit are shown in Table 1.

Table 1. Component values of predistortion circuit.

Name	Value	Unit
Z_o	50	Ω
C_b	500	pF
C_o	300	pF
R_b	20	Ω
R_s	27	Ω
C_d	2.0	pF
V_d	1.5	V

Figure 4(c) shows a photograph of the fabricated predistorter. The input and output connectors were SubMiniature version A connectors. The size of the predistorter was maintained as smaller than 10 mm × 10 mm, excluding the size of the RF and DC connectors. This small size of the predistorter provides a good advantage for the optical transmitter design.

IV. Experiment

We evaluated the performance of the predistorter through the following experiment: Figure 5(a) shows a schematic diagram of an RoF link. Figure 5(b) shows the experimental setup used to measure the gain and phase deviations of the link. The VNA (Agilent N5235A) generated sinusoidal signals at 160 MHz for the S-parameter measurements. To expand the limited output power of the VNA, we inserted a linear RF low-noise amplifier with the output power at a third-order intercept point of 35 dBm and a gain of 15 dB. The experimental setup for this two-tone test (IMD3 measurement) and EVM measurement is shown in Fig. 5(c). The VSG (Rohde & Schwarz SMW200A) two-tone signals were generated at 160 MHz and 170 MHz with 10 MHz spacing. The fabricated predistorter was placed between the VSG and the RoF link. We biased the predistorter at the designed value of 1.5 V. An uncooled DFB laser (Teradian TAD5204) with a center wavelength of 1550 nm was biased at 24 mA. The output optical power of the DFB-LD was 3 dBm. We used a variable optical attenuator to set the

ETRI Journal, Volume 38, Number 2, April 2016
http://dx.doi.org/10.4218/etrij.16.2515.0038

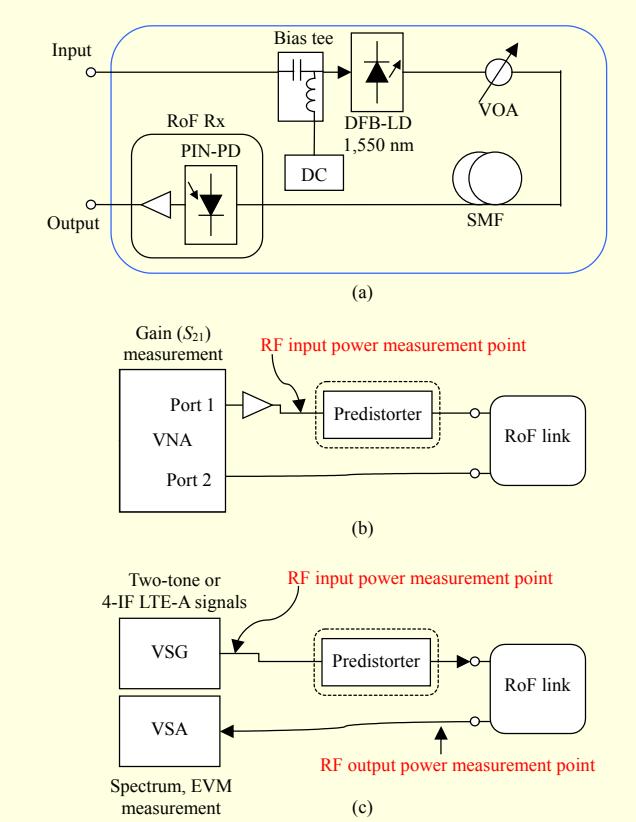

Fig. 5. (a) Schematic diagram of RoF link, (b) experimental setup used to measure gain and phase deviations, and (c) experimental setup for two-tone test and EVM measurement.

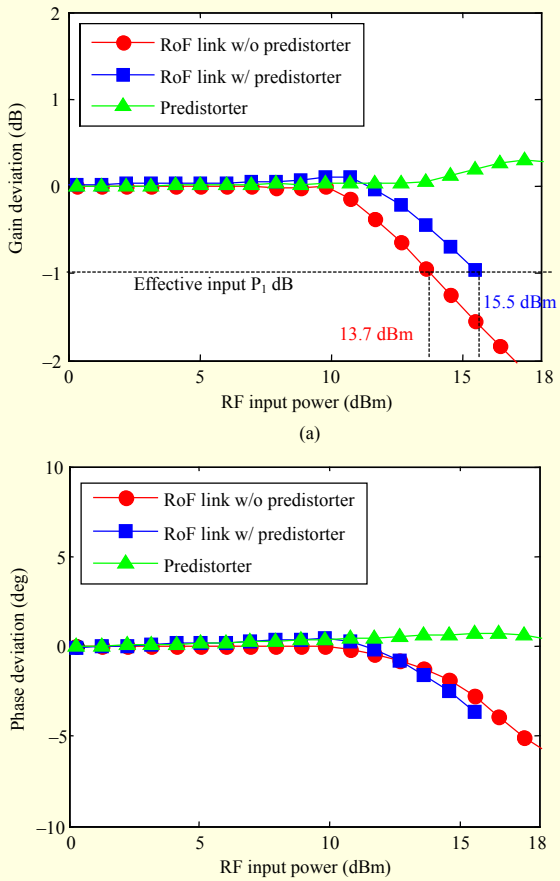

Fig. 6. Measured (a) gain and (b) phase deviations of RoF link with and without predistorter, and predistorter itself.

received optical power at –10 dBm for the receiver PIN-photodiode to prevent nonlinear responses from photocurrent saturation. A vector signal analyzer (VSA, Rohde & Schwarz FSW) was adopted for the spectrum and EVM measurements of the RF signal from the optical receiver. We also conducted a 4-IF carrier transmission of an LTE-A signal across 20 km of SMF. The VSG generated 4 × 20 MHz 64-QAM LTE-A signals. To give some specification relaxation to band-pass filters in the up-and down-conversion processes in the RU, the center frequencies of the IF carriers were assigned starting at 160 MHz with 22 MHz spacing. The total optical loss of the link was set to 10 dB including 20 km SMF and additional loss (for example, WDM couplers) emulations.

The measured gain and phase deviations of the RoF link are shown in Fig. 6. The circles, squares, and triangles show the RoF link with and without a predistorter, and the predistorter itself, respectively. For a clearer understanding, the gains and phases were normalized to be zero in the low input power range in both Figs. 6(a) and 6(b). An insertion loss of 3.8 dB in the predistorter was taken into account for cases with and without a predistorter. It can be seen that the predistorter has a positive gain deviation in Fig. 6(a). The effective input of P_1 dB was improved by 1.8 dB, from 13.7 dBm to 15.5 dBm. We can also confirm a slight negative phase deviation, as shown in Fig. 6(b). The results indicate that the predistorter was able to improve the linearity of the RoF link through a positive gain with an increase in the input RF power.

In most cases for a multi-IFoF link, the multiplexed carriers are equally spaced [4], [5], [10]. In such systems, IMD3 terms between carriers are a dominant factor for limiting the CNDR. Figure 7 describes the IMD3 characteristic of the RoF link with and without the predistorter. The black solid line denotes the theoretical IMD3 values calculated from (6). The hollow and solid symbols represent simulated and measured IMD3 curves, respectively. The RF output power was measured at the fundamental frequencies of 160 MHz and 170 MHz. The simulated curves were derived from the harmonic-balance simulation, which used the AM-AM/PM model of the RoF link. The theoretical, simulated, and measured results show good agreement. It is assumed that the IMD3 reduction is maximized at a certain RF input power, where the IMD3 characteristics of both the predistorter and the RoF link are

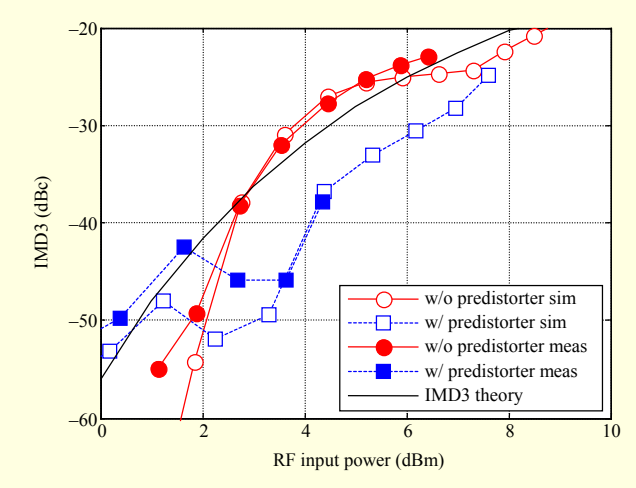

Fig. 7. Simulated (hollow symbols) and measured (solid symbols) IMD3 characteristics of RoF link with and without predistorter. Black solid line represents theoretical IMD3 curve.

similar. The IMD3 of the predistorter is proportional to the RF input power[0]. On the contrary, in a directly modulated RoF system, the IMD3 is not proportional to the RF input power under a large-signal modulation condition [21]. The IMD3 suppression seems not to be constant, because the IMD3 characteristics of the predistorter and the RoF link are different. At RF input power ranges of under 2 dBm, the IMD3 characteristics were worse when the predistorter was implemented owing to the inherent nonlinearity of the predistortion circuit. For an RF input power of greater than 2 dBm, we can confirm an improvement in the IMD3. When the fundamental input power was 3.5 dBm, the IMD3 suppression was as high as 14 dB.

Figure 8 shows the overall EVM and CNDR characteristics for the 4-IF LTE-A carriers versus OMI/ch. The solid curves in Fig. 8(b) are the calculated results of Fig. 3. The circles and squares indicate the RoF link without and with a predistorter, respectively. In Fig. 8(b), the calculated CNDR curve and measured CNDR curve without a predistorter show good agreement when the OMI/ch is lower than 30%. The OMI was calculated from the threshold current and biasing condition of the LD. In Fig. 8(a), the acceptable OMI/ch range has improved from 53% to 71% considering the 3GPP EVM specifications. In other words, we can increase the input dynamic range of the RoF link by 2.54 dB by implementing the predistorter. The constellation diagrams indicate an EVM of 8% and 5.1% without and with the predistorter when the OMI/ch was about 53%, respectively. In Fig. 8(b), the measured CNDR curves show that the predistorter has mitigated the nonlinear distortions caused by clipping. Owing to the implementation of the predistorter, the dynamic range of

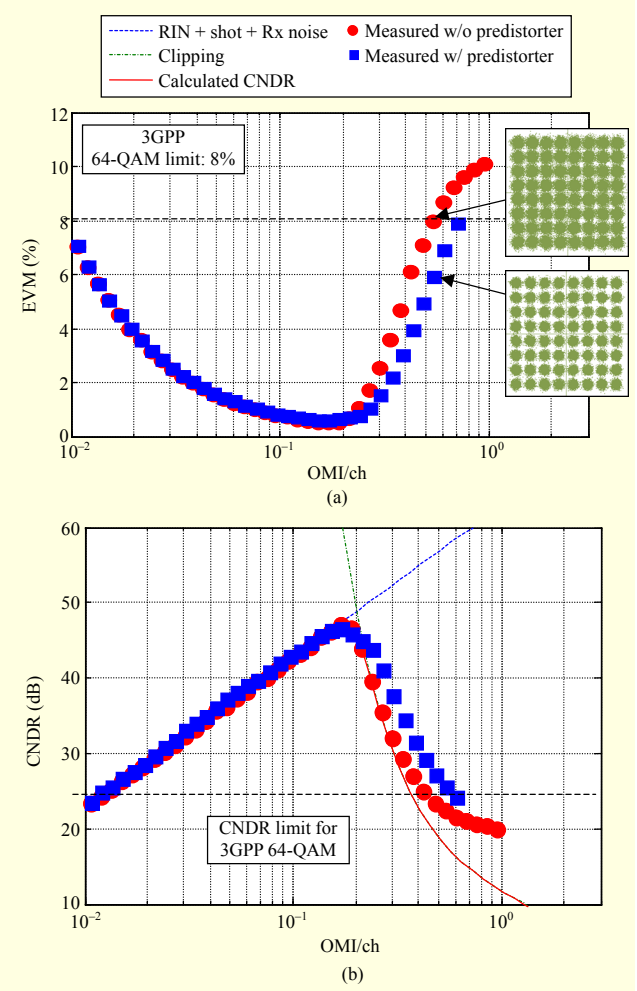

Fig. 8. (a) EVM and (b) CNDR of 4-IF multiplexed LTE-A signals after 20 km optical fiber transmission.

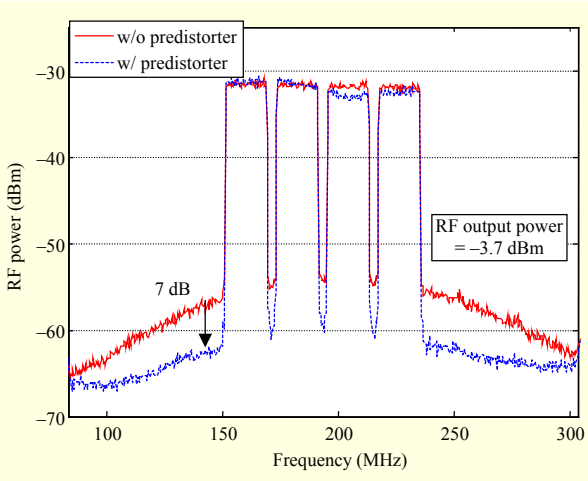

Fig. 9. Received RF spectra of 4-IF LTE-A carriers.

the RoF link improved from 2.1 dB considering the extended OMI/ch range. It infers that the RoF link can accommodate 1.58 times the number of RF carriers using the predistorter.

Figure 9 shows the received RF spectra of the 4-IF LTE-A carriers when the RF output power was −3.7 dBm. The red solid and blue dashed lines indicate the RF spectrum without and with the predistorter, respectively. The resolution bandwidth of the ESA was 100 kHz. The results show that the shunt diode predistorter successfully suppressed 7 dB of the in-band IMD3 components of the RoF link. Alternatively, at the same RoF link gain, we can gain more signal quality by using the predistorter.

V. Conclusion

We reported the clipping distortion suppression of a directly modulated multi-IFoF mobile fronthaul link using a simple shunt diode predistorter. We first analyzed the transmission performance of the directly modulated link and found that the achievable CNDR is limited by the clipping distortion within the high OMI range. To suppress the clipping distortion, we designed a predistortion circuit based on the AM/AM-PM model of an RoF link. The fabricated predistorter provides admirable advantages in transceiver implementation thanks to its simple structure and small dimensions of 10 mm × 10 mm. We also described a demonstration of the fabricated predistorter with an RoF link and confirmed its ability to suppress clipping distortion. The IMD3 of the link was improved by 14 dB, whereas the acceptable OMI/ch range of the 4-IF-multiplexed LTE-A signal was improved by 18%.

References

[1] C.-L. I et al., "Recent Progress on C-RAN Centralization and Cloudification," *IEEE Access*, vol. 2, Aug. 2014, pp. 1030–1039.

[2] Common Public Radio Interface (CPRI), *CPRI Interface Specification V6.1*, 2014.

[3] Open Base Station Architecture (OBSAI), *OBSAI Syst. Specification V2.0*, 2006.

[4] S.-H. Cho et al., "Cost-Effective Next Generation Mobile Fronthaul Architecture with Multi-IF Carrier Transmission Scheme," *Opt. Fiber Commun. Conf.*, San Francisco, CA, USA, Mar. 2014, pp. Tu2B.6.

[5] M. Zhu et al., "High-Capacity Mobile Fronthaul Supporting LTE-Advanced Carrier Aggregation and 8 × 8 MIMO," *Opt. Fiber Commun. Conf.*, Los Angeles, CA, USA, Mar. 2015, pp. M2J.3.

[6] D. Wake, A. Nkansah, and N.J. Gomes, "Radio over Fiber Link Design for Next Generation Wireless Systems," *J. Lightw. Technol.*, vol. 28, no. 16, Mar. 2010, pp. 2456–2464 .

[7] S.-H. Cho et al., "Experimental Demonstrations of Next Generation Cost-Effective Mobile Fronthaul with IFoF Technique," *Opt. Fiber Commun. Conf.*, Los Angeles, CA, USA, Mar. 2015, pp. M2J.5.

[8] X. Liu et al., "Demonstration of Bandwidth-Efficient Mobile Fronthaul Enabling Seamless Aggregation of 36 E-UTRA-Like Wireless Signals in a Single 1.1-GHz Wavelength Channel," *Opt. Fiber Commun. Conf.*, Los Angeles, CA, USA, Mar. 2015, pp. M2J.2.

[9] A.A.M. Saleh, "Fundamental Limit on Number of Channels in Subcarrier-Multiplexed Lightwave CATV System," *Electron. Lett.*, vol. 25, no. 12, June 1989, pp. 776–777.

[10] P. Chiang and W.I. Way "Ultimate Capacity of a Laser Diode in Transporting Multichannel M-QAM Signals," *J. Lightw. Technol.*, vol. 15, no. 10, Oct. 1997, pp. 1914–1924.

[11] B.H. Wang et al., "Large-Signal Spurious-Free Dynamic Range due to Static and Dynamic Clipping in Direct and External Modulation Systems," *J. Lightw. Technol.*, vol. 16, no. 10, Oct. 1998, pp. 1773–1785.

[12] H. Kim and Y.C. Chung, "Passive Optical Network for CDMA-Based Microcellular Communication systems," *J. Lightw. Technol.*, vol. 19, no. 3, Mar. 2001, pp. 301–311.

[13] R. Salmanzadeh and B.M. Tazehkand, "A Modified Method Based on the Discrete Sliding Norm Transform to Reduce the PAPR in OFDM Systems," *ETRI J.*, vol. 36, no. 1, Feb. 2014, pp. 42–50.

[14] L. Roselli et al., "Analog Laser Predistortion for Multiservice Radio-over-Fiber Systems," *J. Lightw. Technol.*, vol. 21, no. 5, 2003, pp. 1211–1223.

[15] T. Ismail et al., "High-Dynamic-Range Wireless-over-Fiber Link Using Feedforward Linearization," *J. Lightw. Technol.*, vol. 25, no. 11, Nov. 2007, pp. 3274–3282.

[16] Y. Pei et al., "Complexity-Reduced Digital Predistortion for Subcarrier Multiplexed Radio over Fiber Systems Transmitting Sparse Multi-Band RF Signals," *Opt. Exp.*, vol. 21, no. 3, 2013, pp. 3708–3714.

[17] C. Han et al., "Linearity Improvement of Directly-Modulated Multi-IF-over-Fiber LTE-A Mobile Fronthaul Link Using Shunt Diode Predistorter," *European Conf. Opt. Commun.*, Valencia, Spain, Sept. 27–Oct. 1, 2015, pp.1–5

[18] 3GPP TS 36.104 v. 11.2.0, *Base Station (BS) Radio Transmission and Reception*, Tech. Spec. Group Radio Access Network, Rel. 11, Nov. 2012.

[19] R.A. Shafik, M.S. Rahman, and A.R. Islam, "On the Extended Relationships among EVM, BER, and SNR as Performance Metrics," *Int. Conf. Elect. Comput. Eng.*, Dhaka, Bangladesh, Dec. 19–21, 2006, pp. 408–411.

[20] K. Yamauchi et al., "A Microwave Miniaturized Linearizer Using a Parallel Diode with a Bias Feed Resistance," *IEEE Trans. Microw. Theory Technol.*, vol. 45, no. 12, Dec. 1997, pp. 2431–2435.

[21] B.H. Wang et al., "Large-Signal Spurious-Free Dynamic Range due to Static and Dynamic Clipping in Direct and External Modulation Systems," *J. Lightw. Technol.*, vol. 16, no. 10, Oct. 1998, pp. 1773–1785.

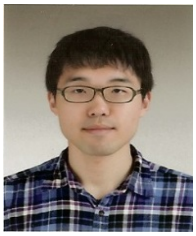

Changyo Han received his BS degree in electrical and electronic engineering from the Tokyo Institute of Technology, Japan, in 2011 and his MS degree in electrical engineering and information systems from the University of Tokyo, Japan, in 2013. In 2013, he joined ETRI. His current research interests are radio-over-fiber technology, coherent optical communication systems, and spatial multiplexing.

Seung-Hyun Cho received his BS and MS degrees in electronic materials engineering from Kwangwoon University, Seoul, Rep. of Korea, in 1997 and 1999, respectively. He received his PhD degree in materials science and engineering from Hanyang University, Seoul, Rep. of Korea, in 2010. From 1999 to 2000, he worked for Access Network Laboratory of Korea Telecom, Daejeon, Rep. of Korea. Since 2000, he has been with ETRI, where he is now a senior researcher. His current research interests are next-generation optical access networks, mobile fronthaul and backhaul networks, and optical-mobile converged access networks.

Minkyu Sung received his BS degree in computer and communication engineering from Korea University, Seoul, Rep. of Korea, in 2010 and his PhD degree in computer and radio communication engineering from Korea University, in 2015. In 2015, he joined ETRI. His current research interests include mobile fronthaul, radio-over-fiber, and optical OFDM.

Hwan Seok Chung received his PhD degree in electronics engineering from the Korea Advanced Institute of Science and Technology (KAIST), Daejeon, Rep. of Korea, in 2003. In 2003, he was a postdoctoral research associate with KAIST, where he worked on hybrid CWDM/DWDM systems for metro area networks. From 2004 to 2005, he was with KDDI R&D laboratories Inc., Saitama, Japan, where he was engaged in research on wavelength converters and regenerators. Since 2005, he has been with ETRI, where he is currently a principal research engineer. His current research interests are mobile fronthaul, high-speed passive optical networks, and modulation formats. He has served as a technical committee member of Optical Fiber Communication Conference (OFC), Optoelectronics and Communications Conference (OECC), Conference on Optical Internet (COIN), and Photonic West. He was the recipient of the best paper awards from the OECC in 2000 and 2003 as well as ETRI in 2011 and 2012. He is also a senior member of the IEEE.

Jong Hyun Lee received his BS, MS, and PhD degrees in electronics engineering from Sungkyunkwan University, Suwon, Rep of Korea, in 1981, 1983, and 1993, respectively. Since 1983, he has been with ETRI, where he has served as a director for both the Optical Communication Department and the Research Strategy & Planning Department. He was also an executive director for the Optical Internet Research Department. His current research interests are packet-circuit-optical converged switching systems, green Internet data center, and optical access networks.

ETRI Journal, Volume 38, Number 2, April 2016
http://dx.doi.org/10.4218/etrij.16.2515.0038